Remarkable resilience of teeth

Herzl Chai[a], James J.-W. Lee[b,c], Paul J. Constantino[b], Peter W. Lucas[b], and Brian R. Lawn[c,1]

[a]School of Mechanical Engineering, Tel Aviv University, Tel Aviv 69978, Israel; [b]Department of Anthropology, George Washington University, Washington, DC 20052; and [c]Ceramics Division, National Institute of Standards and Technology, Gaithersburg, MD 20899-8520

Communicated by John W. Hutchinson, Harvard University, Cambridge, MA, March 5, 2009 (received for review November 20, 2008)

Tooth enamel is inherently weak, with fracture toughness comparable with glass, yet it is remarkably resilient, surviving millions of functional contacts over a lifetime. We propose a microstructural mechanism of damage resistance, based on observations from ex situ loading of human and sea otter molars (teeth with strikingly similar structural features). Section views of the enamel implicate tufts, hypomineralized crack-like defects at the enamel–dentin junction, as primary fracture sources. We report a stabilization in the evolution of these defects, by ''stress shielding'' from neighbors, by inhibition of ensuing crack extension from prism interweaving (decussation), and by self-healing. These factors, coupled with the capacity of the tooth configuration to limit the generation of tensile stresses in largely compressive biting, explain how teeth may absorb considerable damage over time without catastrophic failure, an outcome with strong implications concerning the adaptation of animal species to diet.

dental enamel | evolutionary biology | fracture | microstructure | tufts

Mammalian dental enamel is highly brittle. Yet teeth can withstand high bite forces imposed thousands of times each day during chewing. In humans, these forces can reach up to 1,000 N, and in great apes they can be even higher (1, 2). In contrast to natural crack-resistant laminate structures such as shells and nacre (3, 4), enamel has a toughness close to that of glass (5, 6), making it highly vulnerable to fracture (7, 8). And fracture it does. Vertical cracks or ''lamellae'' are commonly observed in erupted human teeth (9), progressing with age over millions of cycles. How do teeth sustain such cracks without catastrophic failure? Arguably the mammals in which crack-like defects matter most are those that break down hard food objects such as seeds (8, 10–13) and mollusk shells (14, 15). Such mammals include primates (incorporating humans and their hominin ancestors), bears, suoids (pigs and peccaries), and sea otters, each of which has converged on a low-crowned, blunt-cusped class of mammalian molar called ''bunodonty.'' Perhaps the closest evolutionary parallel to hominins in the context of dental morphology are the sea otters (16), a comparison that we advance here to the microstructural level.

Recent studies are revealing how the enamel of bunodont teeth fractures under simulated biting and are providing explicit relations for predicting critical forces for each fracture mode in terms of material properties and tooth/food contact geometry (8, 17). Enamel thickness and cusp size emerge as key dimensions in these models. However, what is the role of the underlying tooth microstructure? The literature on enamel morphology indicates a complex hierarchical structure consisting of bundles of hydroxyapatite nanocrystals within aligned prisms or rods weakly bound by thin protein sheaths (7, 18). The prisms can undulate and cross each other (decussation), much like a basket weave (18, 19). Enamel also contains arrays of intrinsic defects, principally hypocalcified fissures that emanate from the enamel–dentin junction (EDJ). These defects have the characteristics of ''closed cracks'' filled with organic matter, and are known as ''tufts'' for their wavy appearance within the prism microstructure (18, 20, 21). They are now believed to be a primary source of the fractures that ultimately develop in tooth enamel during extended function or overloading (22).

In this work we examine the fundamental nature of tooth resilience, and weakness, by conducting ex situ loading tests on extracted human and sea otter molars and examining the sources of fracture in sections of postloaded specimens. We argue that enamel, although not macroscopically tough, nevertheless contains elements in its geometrical and microstructural complexion that confer a certain damage tolerance on the composite tooth structure. Such damage tolerance has long been argued to be an important factor in the adaptation of mammalian dentition to diet (13, 23). It is also of interest in the context of biomimicry, in which dental researchers look to nature for inspiration in next-generation biomaterials design. We explore these connections further here.

Experiment and Analysis

Although biting forces are essentially compressive, weak tensile ''hoop'' stresses form in the enamel coat and drive cracks around the tooth walls, eventually linking the cuspal surface and cervical margin in a ''longitudinal'' fracture mode (22). Examples are shown in Fig. 1, after overloading at the top surface with a tungsten carbide (WC) rod indenter for a human (*A*) and a sea otter (*B*) molar. Two kinds of fractures are observed in Fig. 1: ''radial–median'' cracks (R), initiating from the near-contact zone and propagating downward around the side walls; and ''margin'' cracks (M), initiating from the cervical base and propagating upward. These same cracks find it difficult to enter the tougher, stress-shielded dentin (6, 24); however, at higher loads they can link up to produce spalling of the enamel away from the dentin (25). The key observation is a substantial increase in load required to drive the cracks from inception to completion; hence the damage tolerance (22). This fracture resistance will be augmented by the filling of any slow growing fissures with organic fluids (9, 26), thereby ''gluing'' the crack walls together (self-healing) (27).

Experiments on slices sawed from extracted human molars reveal principal sources of enamel fracture. The slices were cut parallel to the tooth axis, immediately adjacent to a prominent cusp. The specimens were then loaded normally at the top surface with a rod indenter. Fig. 2 shows side views of the slice before (*A*) and after (*B*) loading. There is clear evidence of tuft extension parallel to the vertical loading direction in this specimen. In some specimens the tufts did not extend at all before failure, up to loads twice that attained in Fig. 2*B*, suggesting that there may be varying degrees of healing from the intrusive protein matter. Observe that several cracks have extended a considerable distance upward, more or less in unison, with one at the center ultimately breaking away from its neighbors upward toward the cuspal surface. This synchronized extension suggests a certain built-in stability and resilience to tooth fracture in normal dental function. Note also the disjointed nature of the extended tufts, indicative of crack inhibition at so-called ''Hunter–Schreger bands'' delineating locations of periodic change in prism orientation

Author contributions: H.C., J.J.-W.L., P.J.C., P.W.L., and B.R.L. designed research; H.C., J.J.-W.L., and P.J.C. performed research; H.C. and J.J.-W.L. analyzed data; and P.W.L. and B.R.L. wrote the paper.

The authors declare no conflict of interest.

[1]To whom correspondence should be addressed. E-mail: brian.lawn@nist.gov.

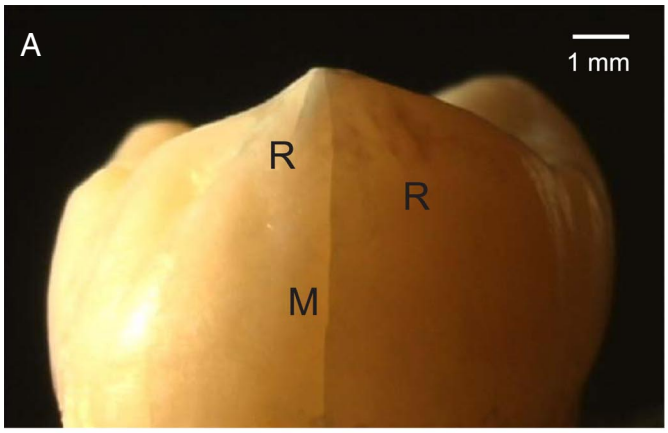

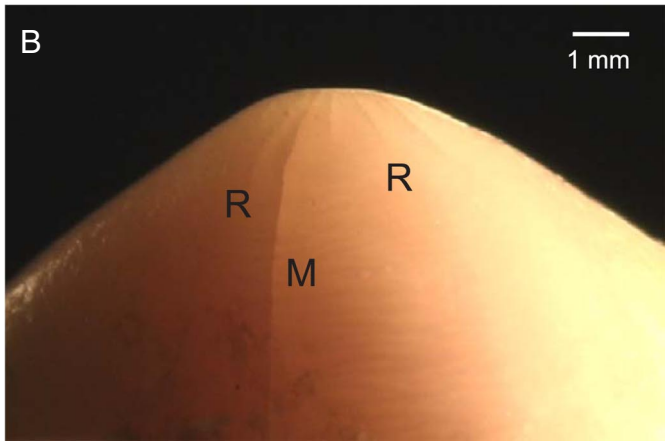

Fig. 1. Fracture of teeth indented along a vertical axis with the flat end of a WC rod. (*A*) Human molar, maximum load 390 N. (*B*) Sea otter molar, maximum load 450 N. Radial–median (R) cracks have propagated part way downward from the contact zone, margin (M) cracks all of the way upward from the cervical base. Some plastic flattening of the indented cusp is evident immediately beneath the indenter.

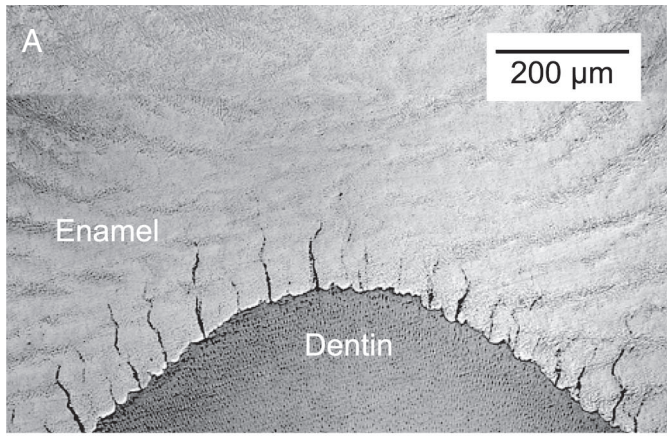

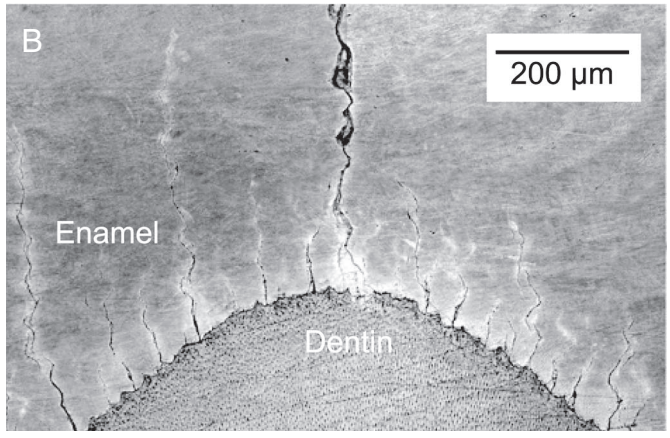

Fig. 2. Optical micrographs showing how cracks grow from tufts at the EDJ in the vicinity of the vertical load axis, in human molar. Specimen is a 1.8-mm-thick longitudinal slice before (*A*) and after (*B*) indentation with WC rod (upper cusp not shown). Cracks in *B* have extended upward from tufts toward the cuspal surface. The faintly visible fringes (Hunter–Schreger bands) mark changes in prism orientation.

(18, 19). Higher magnification views of this segmentation are shown in Fig. 3, for cracks in both human and sea otter teeth.

To quantify the notion of synchronicity in tuft extension, we have conducted a plane-strain finite element analysis for an enamel slice with periodic array of tufts under idealized cuspal loading, corresponding to the specimen geometry of Fig. 2. The tufts were considered as incipient vertical, equispaced cracks of length c and separation w. The contact generates tensile stresses on the cracks, with maximum value σ at the EDJ and decreasing in magnitude along the load axis toward the top surface (28). These stresses fall off relatively slowly around the cusp walls, so adjacent tufts experience similar but slightly diminished fields. Crack driving forces, expressed as "stress intensity factors" K evaluated from the crack-tip displacement fields (29, 30), are plotted in Fig. 4 as a function of normalized crack lengths c/w, for tufts 1, 2, 3, and 4, assuming all tufts to grow at the same value of c (solid curves, with label 1 referring to central tuft). These driving forces show a strong tendency to plateau out with crack extension, indicative of significant stabilization. Also plotted in Fig. 4 are comparative $K(c/w)$ functions for a specimen containing just a single center tuft (i.e., no neighbors) within the same inhomogeneous contact stress field (heavy dashed curve) and within a hypothetical uniform tension stress field σ (light dashed curve). Note that the curve for the single tuft within the contact field still exhibits a plateau, indicating that some of the stabilization must come from the stress field inhomogeneity. The depression in plateau levels for the tufts in the array configuration must be attributable to stress shielding from neighbors. This enhanced stabilization accounts for the multiplicity of steady tuft extensions observed in Fig. 2*B*. Although clearly an oversimplification of the complex loading geometries and microstructural complexions that characterize real tooth chewing function in vivo, this simple model captures the essence of the crack stability.

The same stabilizing phenomenon is apparent in transverse sections of molars, i.e., sections cut normal to the tooth axis. Fig. 5 shows images from a human (*A*) and a sea otter (*B*) molar after loading with a WC rod, at prescribed depths below the contact surface. The images include just a segment of the tooth periphery, with exposed dentin at top. Again, there is indication of synchronized tuft extension into the enamel from the EDJ. Some of these tufts (arrows) extend through the thickness of the enamel to the outer surface. Correlation with postcontact views of the side surface before sectioning reveal the crack outcrops in Fig. 5*A* to coincide with traces of margin cracks and in Fig. 5*B* with radial cracks, again implicating tufts as sources of failure.

A simple experiment was conducted to confirm the crack-like nature of the tufts. Fig. 6 shows scanning electron micrographs of Vickers indentations placed adjacent to (*A*) a tuft and (*B*) a margin crack in a transverse section of a human molar. After applying the contact load, but before sectioning, this specimen was aged in water for 1 week and then allowed to dry. Fig. 6*A* shows a corner crack CC′ from one such Vickers indentation

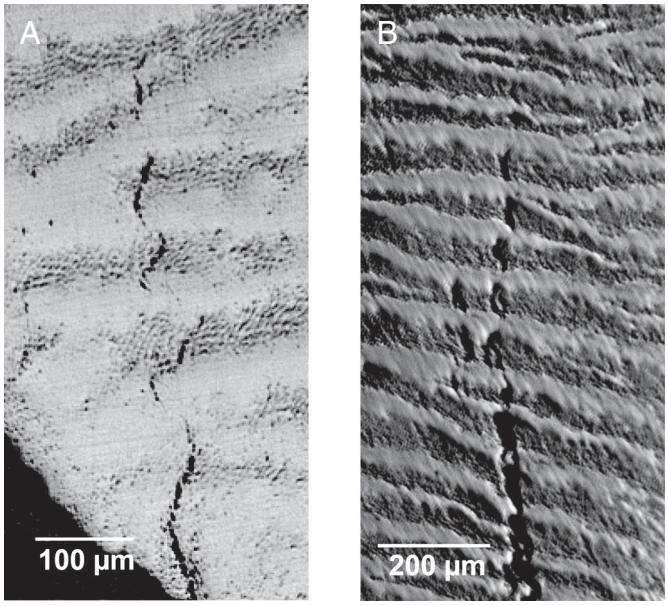

Fig. 3. Optical micrographs from longitudinal sections of human (*A*) and sea otter (*B*) molars, showing disruption of cracks at Hunter–Schreger bands. (*A*) Location of field of view is near EDJ, immediately adjacent to the tooth axis. (*B*) Field of view is ≈2 mm below the cusp surface, midway between EDJ and outer enamel surface.

intersecting a tuft interface TT′ (31). The tuft appears as a closed interface [i.e., filled with matter, presumably largely organic (9, 32)], whereas the corner crack appears as an open interface (apart from some dislodged enamel fragments). In this example, the intersected tuft has delaminated from the lower wall of the interface, confirming it as a weak path within the structure (33). In other cases (notably for more remote indentations), the tuft simply arrested the impinging corner crack without delamination, and in still others the corner crack penetrated the interface and extended into the adjacent enamel. These observations indicate that the filler material provides some degree of protective interfacial bonding, with resultant inhibition of tuft extension. Fig. 6*B* shows an analogous Vickers corner crack CC′ intersecting an aged margin crack MM′, in the same transverse section as in Fig. 6*A*. In this case, the crack has penetrated the interface, indicating that organic material has intruded and solidified during aging, much as in the case of tufts. Corner cracks placed adjacent to newly formed margin cracks without aging in water always arrested at the interface.

Discussion

The present evidence suggests that the strategy of tooth survival is one of damage containment rather than avoidance. Tufts at the EDJ, although agents of weakness, are structured in arrays that provide internal shielding from applied stresses. Thus, it is easy to initiate fractures within the enamel but difficult to drive these fractures to failure. Crack extension may be expected to progress steadily during a lifetime, which would explain why the dentition of older animals, including humans, tends to contain a population of visible crack-like defects (26). Because the process is gradual, the cracks will be continually replenished with protein-rich fluids, thereby slowing propagation even further by a mechanism of self-healing similar to that observed in glass and other brittle materials (27). It is perhaps curious that although tufts have long been documented in the literature on dental histology (18), their potential role as sources of progressive damage has been totally overlooked. Decussation appears to offer some resistance to crack extension from the tufts, by a

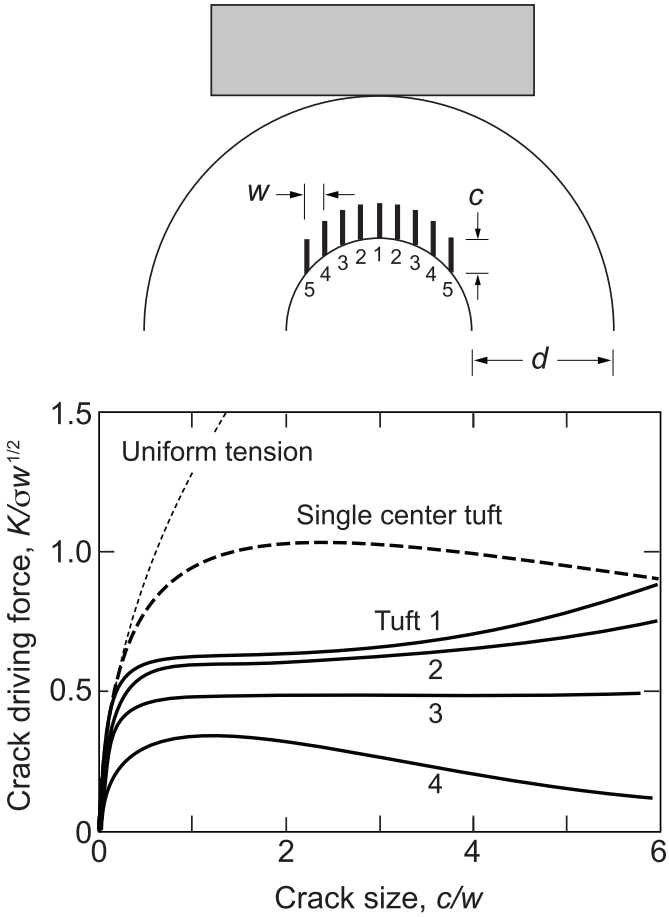

Fig. 4. FEA calculations of stress intensity factor *K* as function of reduced crack size *c*/*w*, for extension of periodic array of cracks in curved bilayer slice. Solid curves are calculations for crack arrays in inhomogeneous contact stress field, with *w*/*d* = 0.1 mm/1.8 mm = 0.055. Heavy dashed curve is for single crack in same stress field. Light dashed curve is for same single crack under uniform stress σ.

mechanism of stepwise crack arrest and penetration/reinitiation across the Hunter–Schreger bands, accounting for the waviness of the extended tufts. The toughness of enamel is >3 times greater than that of constituent hydroxyapatite crystallites within the prisms (34). The fracture patterns in Fig. 3 are reminiscent of those in brittle cross-ply laminate composites (35). Decussation occurs in different degrees in different animals but generally with higher densities in the regions of the EDJ where the tufts originate (8). This implied resistance would appear to compensate somewhat for the intrinsic weakness of the interprism paths; without it, the toughness on pathways parallel to the prisms would be even lower than that of glass. The toughness of human enamel for crack paths perpendicular to the prisms is considerably higher relative to paths parallel to the prisms (5, 6), making enamel more resistant to potentially deleterious lateral chipping (36).

The relationship of tooth form to diet remains a crucial issue in mammalian evolution. Such an understanding is vital to paleontologists and paleoanthropologists because teeth constitute a large portion of the fossil record (13). Arguments have been made asserting that such critical elements as enamel thickness, and to some extent tooth size, act as optimal organizations to frustrate tooth failure in relation to diet (8, 13, 17, 22, 37–39). However, it would seem that enamel microstructure, and especially tufts, are also important factors. The presence of tufts would appear to be a common feature of animal dentition,

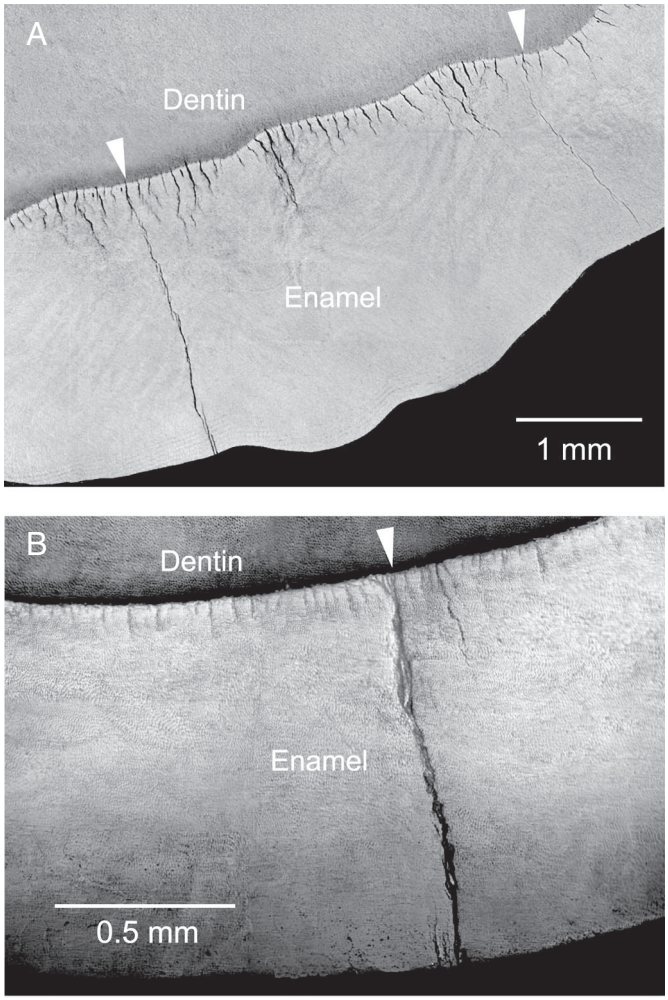

Fig. 5. Segment of transverse section view through molars. (*A*) Human, loaded to 450 N and sectioned to depth 4.4 mm below the cuspal surface. (*B*) Sea otter, loaded to 550 N and sectioned to depth 2.2 mm. Dentin is exposed at top of field of view. Cracks (arrows) appear to initiate from tufts.

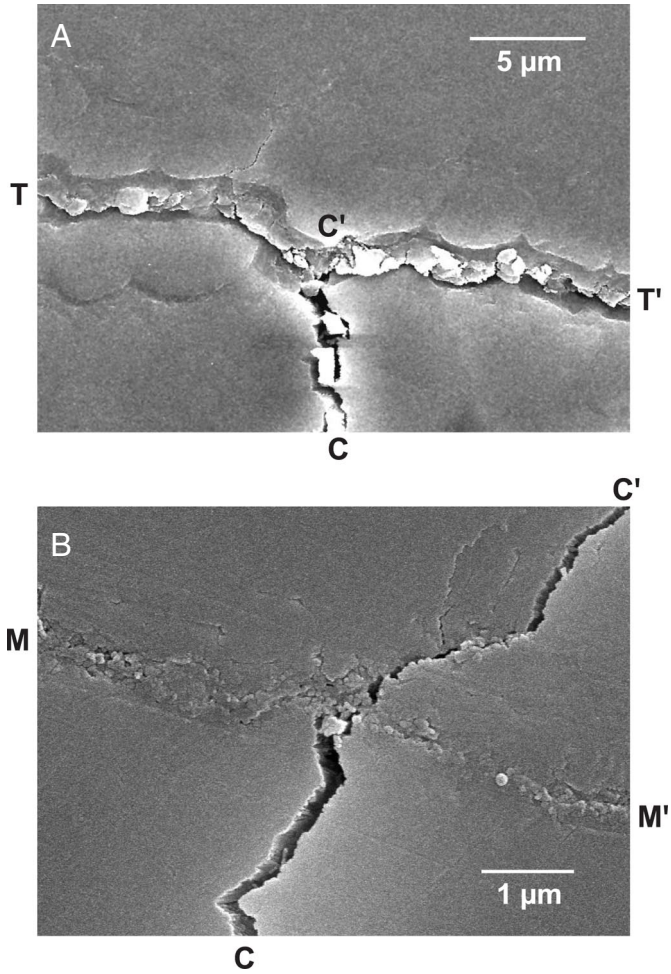

Fig. 6. Scanning electron micrographs from transverse section of human molar, showing intersection of Vickers corner crack CC′ with (*A*) tuft TT′, showing delamination at lower tuft interface along C′T and C′T′, and (*B*) margin crack MM′, showing penetration through interface to adjacent enamel.

especially in primates: we have observed similar structures in enamel sections from chimps, orangutans, and gorillas. Apart from their role in stress shielding, tuft arrays may protect the dentin by increasing the local enamel compliance, effectively "grading" the material properties in the region of the EDJ (40). It is thus likely that the damage tolerance conferred by these defects is intricately tied to tooth morphology and function along the evolutionary path. The specific nature of the cuspal loading is another factor in determining which ensuing damage mode will dominate, and this in turn depends on diet. For chewing on small hard particulates, the principal damage mode is wear in the cuspal zone (8). Because wear is a local process relating to asperity contact at the external surface, tuft configurations and decussation within the enamel interior would be unlikely to confer much benefit. For feeding on large objects, such as nuts and seeds, the greater threat is from longitudinal fracture (8, 17). It is noteworthy that mammals that consume large hard foods, including some primates, sea otters, and giant pandas, tend to show significant decussation in the inner sections of their tooth enamel (41). In these cases, stress shielding, internal fissure self-healing, and prism decussation adjacent to the EDJ, in conjunction with thick enamel and large cuspal radius, offer built-in protection against catastrophic failure from dietary stresses.

Scientists in various disciplines may draw from the findings reported here. For the large body of biologists concerned with the evolution of teeth, our findings suggest that largely overlooked intrinsic structures like tufts may play a vital role in the interplay between internal weakness of enamel and damage tolerance of the integrated tooth structure. Do all enamels possess these features, or are they linked predominantly to bunodonty? For those biomaterials researchers who look to biomimicry for inspiration in the design of synthetic enamel replacements (as well as of bone and soft tissue), the replication of hierarchical fibrous microstructures incorporating weak internal interfaces presents a fascinating challenge. Bioinspired laminate structures that make use of weak internal interfaces to confer toughness, analogous to shells and nacre, constitute just one example of this design philosophy (42). To make any use of such biomimicry, it is crucial that we first understand the underlying micromechanics that determine the structural resilience. Unlike most artificial structures, mammalian systems have a natural inbuilt capacity for self-healing, in the present case from protein-rich fluids in the dentition, that will tend to mitigate susceptibility to cyclic fatigue. Even this last element lies within the realms of possibility, as has been demonstrated by incorporation of microcapsulated crack-release healing agents into polymer microstruc-

tures (43). The future development of such damage-tolerant structures rests with the next generation of innovators.

Materials and Methods

Human molar and premolar teeth for testing were provided by Gary Schumacher and Sabine Dickens of the American Dental Association (ADA) laboratories at the National Institute of Standards and Technology (NIST). The teeth were extracted from male and female patients 18–25 years old and stored in aqueous solution. Intact specimens were selected and cleaned by Anthony Guiseppetti at the ADA. Cursory examination of the surfaces of the as-received teeth revealed the preexistence of crack-like defects of various lengths extending from the cervical–enamel margins longitudinally toward the cuspal area. The average tooth width was 10 mm and crown height 7.5 mm. Approval to test these specimens was granted by the NIST Internal Review Board. The specimens were contained in aqueous solution after receipt and were kept moist during subsequent preparation and testing. Sea otter molar and premolar teeth were supplied by Jim Estes and Nate Dominy of the University of California at Santa Cruz (UCSC). These were from the skulls of deceased animals that had been dissected, cleaned, and frozen by Andy Cunningham at UCSC before shipping to us in a dry state. Permission to transport and test the sea otter teeth was granted by Melissa Miller of the California Department of Fish and Game. Upon receipt, the teeth were extracted from the mandibles and stored in water. All remains of these animals are ultimately to be lodged at the California Academy of Sciences.

The photos of human and otter molars in Fig. 1 were obtained from specimens after subjection to a compression fracture test (17). Individual teeth were mounted with their roots embedded in epoxy blocks, cusps uppermost. The mounted specimens were placed onto the platform of a mechanical testing machine and kept moist during testing by continually squirting drops from a water bottle. A flat tungsten carbide rod was used to apply a vertical load to the most prominent cusp of each tooth. A video camera was used to view the progress of the cracks in situ around the buccal or lingual walls immediately adjacent to the indented cusp during the loading. Oblique lighting was adjusted to provide optimum contrast at the fracture sites.

Sections through the teeth were made by conventional grinding and polishing. Images of the sections were obtained by using reflection optical microscopy and scanning electron microscopy. The longitudinal slices in Figs. 2 and 3 were cut using a diamond saw. Two cuts 1.5 mm apart were made either side of a selected cusp, parallel to the prospective vertical load axis. The resulting faces were polished to 1-μm finish with diamond paste. The slices were then mounted into epoxy blocks and loaded with a tungsten carbide rod, as described above. Again, a video camera was used to photograph the tuft responses in the region of the EDJ. The transverse tooth sections in Figs. 5 and 6 were prepared by serial grinding and polishing of indented specimens, once more to 1-μm finish. These sections were polished to prescribed depths below the indented cusp.

Finite element analysis (FEA) was used to determine stress intensity factors for the crack array shown in Fig. 4 *Inset*. A mesh was set up for a curved enamel/dentin bilayer slice of depth 1.5 mm, with enamel thickness $d = 1.8$ mm and outer radius 3 mm, by using a commercial ANSYS finite element package. Young's modulus and Poisson's ratio were taken as 90 GPa and 0.22 for enamel, 18 GPa and 0.35 for dentin. Some 9 cracks of size c and spacing $w = 0.1$ mm were incorporated into the enamel coat, labeled 1, 2, 3, 4, and 5 as shown. A concentrated load was then applied at the top of the cusp by a rigid flat indenter. The mesh was scaled to smaller grid size in the vicinity of the crack tips, and the configuration was refined until the solutions reached convergence. The displacement fields near the tip of the cracks were thus determined, from which the stress intensity factor K, a measure of the generalized force driving the crack, was deconvoluted by using standard fracture mechanics (44). Calculations of K were made for each crack at specified values of c (same for all cracks) with w held fixed, and the curves in Fig. 4 were thereby generated. Comparative calculations were made for a single center tuft in the absence of any neighbors, within the same contact stress field and within a hypothetical uniform stress, to separate contributions to crack stability from stress field inhomogeneity and near-neighbor shielding.

ACKNOWLEDGMENTS. We thank Sangwon Myoung for assistance with specimen preparation. This work was supported by the George Washington University Research Enhancement Fund (to P.J.C.).

1. Lucas PW, Peters CR, Arrandale S (1994) Seed-breaking forces exerted by orangutans with their teeth in captivity and a new technique for estimating forces produced in the wild. *Am J Phys Anthropol* 9:365–378.
2. Braun S, et al. (1995) A study of bite force. 1. Relationship to various physical characteristics. *Angle Orthodontist* 65:367–372.
3. Kamat S, Su X, Ballarini R, Heuer AH (2000) Structural basis for the fracture toughness of the shell of the conch *Strombus gigas*. *Nature* 405:1036–1040.
4. Evans AG, et al. (2001) Model for the robust mechanical behavior of nacre. *J Mater Res* 16:2475–2484.
5. Rasmussen ST, Patchin RE, Scott DB, Heuer AH (1976) Fracture properties of human enamel and dentin. *J Dent Res* 55:154–164.
6. Xu HHK, et al. (1998) Indentation damage and mechanical properties of human enamel and dentin. *J Dent Res* 77:472–480.
7. Maas MC, Dumont ER (1999) Built to last: The structure, function, and evolution of primate dental enamel. *Evol Anthropol* 8:133–152.
8. Lucas PW, Constantino PJ, Wood BA, Lawn BR (2008) Dental enamel as a dietary indicator in mammals. *BioEssays* 30:374–385.
9. Sognnaes RF (1950) The organic elements of enamel. IV. The gross morphology and the histological relationship of the lamellae to the organic framework of the enamel. *J Dent Res* 29:260–269.
10. Jolly CJ (1970) The seed-eaters: A new model of hominid differentiation based on a baboon analogy. *Man* 5:5–26.
11. Kiltie RA (1982) Bite force as a basis for niche differentiation between rain-forest peccaries (*Tayassu tajacu* and *Tayassu pecari*). *Biotropica* 14:188–195.
12. Peters CR (1987) Nut-like oil seeds: Food for monkeys, chimpanzees, humans, and probably ape-men. *Am J Phys Anthropol* 73:333–363.
13. Lucas PW (2004) *Dental Functional Morphology*: *How Teeth Work* (Cambridge Univ Press, Cambridge, UK).
14. Murie OJ (1940) Notes on the sea otter. *J Mammol* 21:119–131.
15. Fisher EM (1941) Notes on the teeth of the sea otter. *J Mammol* 22:428–433.
16. Walker AC (1981) Diet and teeth: Dietary hypotheses and human evolution. *Phil Trans R Soc London* B 292:57–64.
17. Lawn BR, Lee JJ-W, Constantino PJ, Lucas PW (2009) Predicting failure in mammalian enamel. *J Mech Behav Biomed Mat* 2:33–42.
18. Osborn JW (1981) Dental tissues. *Dental Anatomy and Embryology*, ed Osborn JW (Blackwell, Oxford), Vol 1, pp 155–209.
19. Koenigswald WV, Rensberger JM, Pretzschner HU (1987) Changes in the Tooth enamel of early Paleocene mammals allowing increased diet diversity. *Nature* 328:159–162.
20. Sognnaes RF (1949) The organic elements of enamel. II. The organic framework of the internal part of the enamel, with special regard to the organic basis for the so-called tufts and Schreger bands. *J Dent Res* 28:549–557.
21. Osborn JW (1969) The 3-dimensional morphology of the tufts in human enamel. *Acta Anat* 73:481–495.
22. Lee JJ-W, et al. (2009) Fracture modes in human teeth. *J Dent Res* 88:224–28.
23. Janis CM, Fortelius M (1988) On the means whereby mammals achieve increased functional durability of their dentitions, with special reference to limiting factors. *Biol Rev Cambridge Philos Soc* 63:197–230.
24. Imbeni V, Kruzic JJ, Marshall GW, Marshall SJ, Ritchie RO (2005) The dentin–enamel junction and the fracture of human teeth. *Nature Mat* 4:229–232.
25. Popowics TE, Rensberger JM, Herring SW (2004) Enamel microstructure and microstrain in the fracture of human and pig molar cusps. *Arch Oral Biol* 49:595–605.
26. Bodecker CF (1953) Enamel lamellae and their origin. *J Dent Res* 32:239–245.
27. Roach DH, Lathabai S, Lawn BR (1988) Interfacial layers in brittle cracks. *J Am Ceram Soc* 71:97–105.
28. Rudas M, Qasim T, Bush MB, Lawn BR (2005) Failure of curved brittle layer systems from radial cracking in concentrated loading. *J Mater Res* 20:2812–2819.
29. Tada H, Paris P, Irwin GR (1985) *The Stress Analysis of Cracks Handbook* (Del Research, St Louis), p 15.1.
30. Fett T, Munz D (1997) *Stress Intensity Factors and Weight Functions* (Computational Mechanics, Southampton, UK), pp 267–268.
31. Kim J-W, Bhowmick S, Hermann I, Lawn BR (2006) Transverse fracture of brittle layers: Relevance to failure of all-ceramic dental crowns. *J Biomed Mater Res* 79B:58–65.
32. Palamara J, Phakey PP, Rachinger WA, Orams HJ (1989) The ultrastructure of spindles and tufts in human dental enamel. *Adv Dent Res* 3:249–257.
33. He M-Y, Hutchinson JW (1989) Crack deflection at an interface between dissimilar elastic materials. *Int J Solids Struct* 25:1053–1067.
34. Bajaj D, Nazari A, Eidelman N, Arola DD (2008) A comparison of fatigue crack growth in human enamel and hydroxyapatite. *Biomaterials* 29:4847–4854.
35. Xia ZC, Carr RR, Hutchinson JW (1993) Transverse cracking in fiber-reinforced brittle matrix, cross-ply laminates. *Acta Mater* 41:2365–2376.
36. Kim J-W, Bhowmick S, Chai H, Lawn BR (2007) Role of substrate material in failure of crown-like layer structures. *J Biomed Mater Res* 81B:305–311.
37. Martin L (1985) Significance of enamel thickness in hominoid evolution. *Nature* 314:260–263.
38. Teaford MF, Ungar PS (2000) Diet and the evolution of the earliest human ancestors. *Proc Natl Acad Sci USA* 97:13506–13511.
39. Humphrey LT, Dean MC, Jeffries TE, Penn M (2008) Unlocking evidence of early diet from tooth enamel. *Proc Natl Acad Sci USA* 105:6834–6839.
40. Cuy JL, Mann AB, Livi KJ, Teaford MF, Weihs TP (2002) Nanoindentation mapping of the mechanical properties of human molar tooth enamel. *Arch Oral Biol* 7:281–291.
41. Stefen C (1999) Enamel microstructure of recent and fossil Canidae (Carnivora: Mammalia). *J Verteb Paleontol* 19:576–587.
42. Munch E, et al. (2008) Tough, bio-inspired hybrid materials. *Science* 322:1516–1520.
43. White SR, et al. (2001) Autonomic healing of polymer composites (2001) *Nature* 409:794–797.
44. Lawn BR (1993) *Fracture of Brittle Solids* (Cambridge Univ Press, Cambridge, UK), pp 16–50.